

Semantic Image Synthesis via Diffusion Models

Weilun Wang¹, Jianmin Bao^{2*}, Wengang Zhou^{1,4},
Dongdong Chen³, Dong Chen², Lu Yuan³, Houqiang Li^{1,4}

¹ CAS Key Laboratory of GIPAS, EEIS Department, University of Science and Technology of China (USTC)

² Microsoft Research Asia ³ Microsoft Cloud+AI

⁴ Institute of Artificial Intelligence, Hefei Comprehensive National Science Center

wwlustc@mail.ustc.edu.cn, {jianbao, dochen, doch, luyuan}@microsoft.com, {zhwg, lihq}@ustc.edu.cn

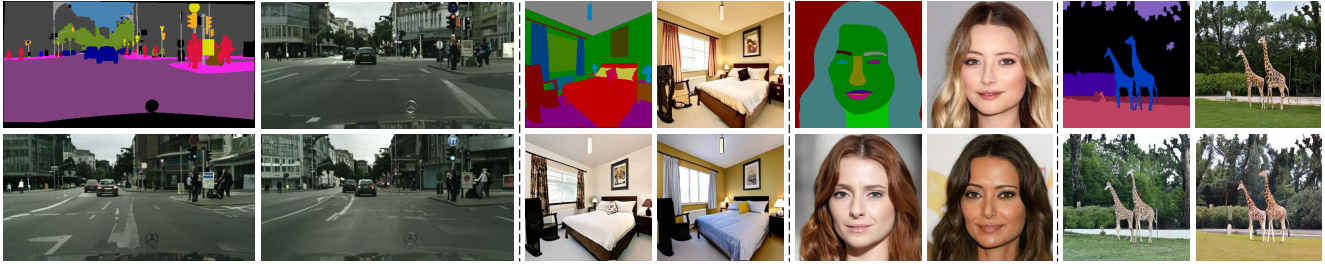


Figure 1. Semantic image synthesis results of our framework on four datasets. The left-top one is the input mask, the left three are the generated images from our framework, our framework generates realistic and diverse images under different scenes.

Abstract

Denosing Diffusion Probabilistic Models (DDPMs) have achieved remarkable success in various image generation tasks compared with Generative Adversarial Nets (GANs). Recent work on semantic image synthesis mainly follows the de facto GAN-based approaches, which may lead to unsatisfactory quality or diversity of generated images. In this paper, we propose a novel framework based on DDPM for semantic image synthesis. Unlike previous conditional diffusion model directly feeds the semantic layout and noisy image as input to a U-Net structure, which may not fully leverage the information in the input semantic mask, our framework processes semantic layout and noisy image differently. It feeds noisy image to the encoder of the U-Net structure while the semantic layout to the decoder by multi-layer spatially-adaptive normalization operators. To further improve the generation quality and semantic interpretability in semantic image synthesis, we introduce the classifier-free guidance sampling strategy, which acknowledge the scores of an unconditional model for sampling process. Extensive experiments on four benchmark datasets demonstrate the effectiveness of our proposed method, achieving state-of-the-art performance in terms of fidelity (FID) and diversity (LPIPS). The code and models are publicly available at <https://github.com/WeilunWang/semantic-diffusion-model>.

1. Introduction

Semantic image synthesis aims to generate photo-realistic images based on semantic layouts, which is a reverse problem of semantic segmentation. This problem can

be widely used in various applications, *i.e.*, image editing, interactive painting and content generation. Recent work [24, 31, 41, 44, 46, 48] mainly follows the adversarial learning paradigm, where the network is trained with adversarial loss [9], along with a reconstruction loss. By exploring the model architectures, these methods gradually improve performance on the benchmark datasets. However, existing GAN-based approaches show limitations on some complex scenes in terms of generating high-fidelity and diverse results.

Denosing diffusion probabilistic models (DDPMs) [11] is a new class of generative model based on maximum likelihood learning. DDPMs generate samples from standard Gaussian distribution to samples of an empirical distribution by an iterative denoising process. With the help of progressive refinement of the generated results, they achieve state-of-the-art sample quality on a number of image generation benchmarks [8, 10, 11].

In this paper, we present the first attempt at exploring diffusion model for the problem of semantic image synthesis and design a novel framework named Semantic Diffusion Model (SDM). The framework follows the denosing diffusion paradigm, transforming the sampled Gaussian noise into a realistic image through an iterative denoising process (see Figure 2). The generation process is a parameterized Markov chain. In each step, the noise is estimated from the input noisy image by a denoising network conditioned on the semantic label map. According to the estimated noise, a less noisy image is generated by the posterior probability formulation. Through iteration, the denoising network progressively produces semantic-related content and injects it into the stream to generate realistic images.

We revisit the previous conditional DDPMs [35, 36]

*Corresponding author: Jianmin Bao.

that directly concatenate the condition information with the noisy image as input of the denoising network. The approach does not fully leverage the information in the input semantic mask, which leads to generated images in low quality and semantic relevance as suggested in previous work [31]. Motivated by this, we design a conditional denoising network which processes semantic layout and noisy image independently. The noisy image is fed into the encoder of the denoising network while the semantic layout is embedded into the decoder of the denoising network by multi-layer spatially-adaptive normalization operators. This highly improves the quality and semantic correlation of generated images.

Furthermore, diffusion model are inherently capable of generating diverse results. The sampling strategy plays an important role in balancing quality and diversity of the generated results. The naïve sampling procedure can generate images that demonstrate high diversity but lack the realism and strong correspondence with semantic label maps. Inspired by [13], we adopt the classifier-free guidance strategy to boost image fidelity and semantic correspondence. Specifically, we fine-tune the pre-trained diffusion model by randomly removing the semantic mask input. Then the sampling strategy is processed based on both the predictions from diffusion model with and without semantic mask. By interpolating the scores from these two situations, the sampling results achieve a higher fidelity and stronger correlation with the semantic mask input.

To demonstrate the superiority of our framework, we conduct experiments on four benchmark datasets, *i.e.*, Cityscapes, ADE20K, CelebAMask-HQ and COCO-Stuff. Both quantitative and qualitative results validates that our framework can generate both high-fidelity and diverse results, achieving superior performance compared with previous methods. Some example results are shown in Figure 1.

Overall, the contributions are summarized as follows:

- We propose a novel framework called **Semantic Diffusion Model** based on DDPMs, for high-fidelity and diverse semantic image synthesis.
- We find the network structure of current conditional diffusion models show limitation in handling the noisy input and semantic masks. We propose a new structure to handle noisy input and semantic mask separately and precisely.
- To achieve better sampling results in diffusion process, we introduce the classifier-free guidance, which yields significantly higher quality and semantic input correlated results.
- Extensive experiments on four benchmark datasets demonstrate the effectiveness of the proposed framework, achieving new state-of-the-art performance on generation fidelity (FID) and diversity (LPIPS).

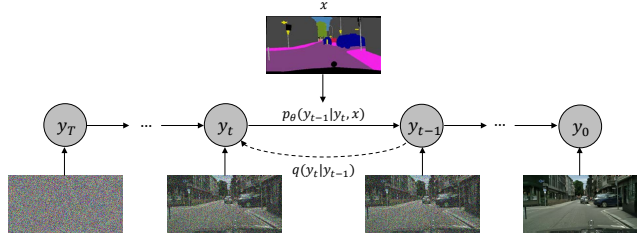


Figure 2. **Conditional Diffusion Model for Semantic Image Synthesis.** The framework transforms the noise from standard Gaussian distribution to the realistic image through iterative denoising process. In each denoising step, we use a U-net-based network to predict noise involved into the noisy images y_t under the guidance of the semantic layouts x .

2. Related Work

In this section, we briefly review the related topics, including denoising diffusion probabilistic models and semantic image synthesis.

2.1. Denoising diffusion probabilistic models.

A diffusion probabilistic model [39] is a parameterized Markov chain that optimizes the lower variational bound on the likelihood function to generate samples matching the data distribution. The diffusion probabilistic model is efficient to define and train but is incapable of generating high-quality samples before. Ho *et. al.* [11] first combine the diffusion probabilistic model with the score-based model and propose the denoising diffusion probabilistic model, which achieves great success in image generation. After that, more and more researchers [1, 8, 12, 18, 19, 30, 37, 40] turn their attention to DDPMs. Notably, Dhariwal and Nichol [8] show the potential of DDPMs, achieving image sample quality superior to GANs, on unconditional image generation.

Recently, conditional DDPMs [2, 6, 10, 16, 17, 21, 27, 29, 35, 36, 38] are studied to develop the application on downstream tasks. Saharia *et. al.* [36] achieve success in super resolution with DDPM. Pattle [35] explores DDPM on four image-to-image translation problems, *i.e.*, colorization, inpainting, uncropping, and JPEG decompression. Bahjat *et. al.* [16] propose an unsupervised posterior sampling method, *i.e.*, DDRM, to solve any linear inverse problem with a pre-trained DDPM. Two concurrent works [10, 29] apply DDPMs for text-to-image generation. However, the aforementioned methods mainly focus on low-level computer vision tasks or work on single dimensional conditions. Differently, we investigate conditional DDPM on generation problem with high-level dense semantic condition.

2.2. Semantic Image Synthesis.

Semantic image synthesis [5, 14, 15, 22–26, 31, 32, 41, 43–48, 50, 56, 57] transforms semantic layouts into diverse realistic images. Recent work on semantic image synthesis is GAN-based and trained with the adversarial loss along with

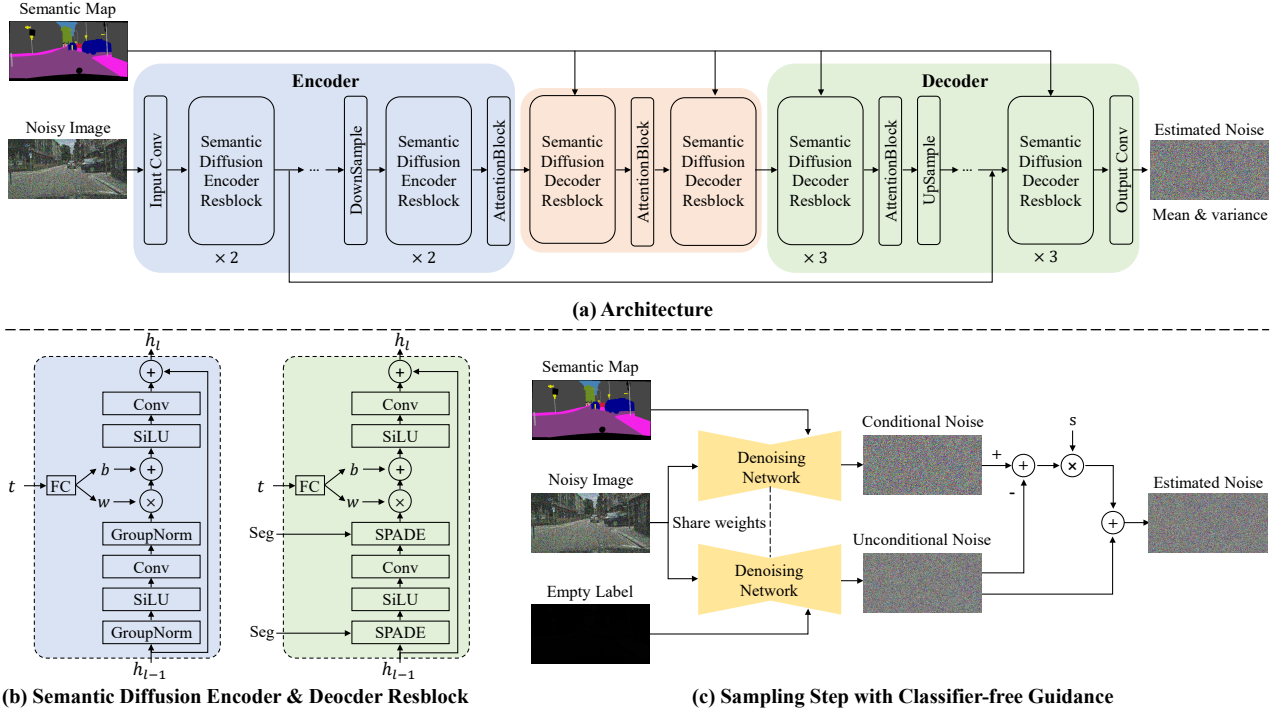


Figure 3. (a) Architecture of conditional denoising network. The denoising network takes the noisy image as input and estimates the involved noise under the guidance of the semantic label map. (b) The detailed structure of semantic diffusion encoder and decoder resblock. (c) The sampling procedure with classifier-free guidance.

the reconstruction loss. Pix2PixHD [48] utilizes a multi-scale generator to produce high-resolution images from semantic label maps. SPADE [31] proposes spatially-adaptive normalization to better embed the semantic layouts into the generator. CLADE [43] further improves the efficiency of SPADE by proposing a new class-adaptive normalization layer. SCGAN [50] introduces a dynamic weighted network for semantic relevance, structure and detail synthesis.

The aforementioned methods mainly focus on generating real and semantically-corresponding unimodal result. Paralleled with these methods, some other methods [14, 42, 55, 57] explore multimodal generation, which is also a core target for one-to-many problems like semantic image synthesis. To tackle this issue, BicycleGAN [55] encourages bidirectional mapping between the generated image and latent code, and DSCGAN [14] propose a simple regularization loss to penalize the generator from mode collapse. More recently, INADE [42] proposes a framework that supports diverse generation at the instance level by instance-adaptive stochastic sampling. However, these multimodal methods still fail to obtain satisfactory results on generation quality and learned correspondence. It is non-trivial for existing GAN-based methods to achieve high generation fidelity and diversity at the same time. To this end, we explore a new kind of approach to semantic image synthesis, *i.e.*, conditional denoising diffusion probabilistic model, and achieve both better fidelity and diversity.

3. Methodology

In this paper, we present a novel framework named Semantic Diffusion Model (SDM) based on DDPMs to transform semantic layouts into realistic images (see Figure 2). With the iterative refinement, our framework generates high-quality images with fine-grained details. The multimodal generation is also supported and the generation results exhibit high diversity, which benefits from the randomness continuously involved by noise at each step. The rest of this section is organized as follows: We begin with reviewing previous conditional denoising diffusion probabilistic models. After that, we outline the architecture and objective functions of the semantic diffusion model. Finally, we present the classifier-free guidance adopted during inference.

3.1. Preliminaries

We first briefly review the theory of conditional denoising diffusion probabilistic models. Conditional diffusion models aims to maximize the likelihood $p_\theta(\mathbf{y}_0|\mathbf{x})$ while the conditional data distribution follows $q(\mathbf{y}_0|\mathbf{x})$. In conditional DDPM, two processes are defined, *i.e.* the reverse process and the forward process. The reverse process $p_\theta(\mathbf{y}_{0:T}|\mathbf{x})$ is defined as a Markov chain with learned Gaussian transitions beginning with $p(\mathbf{y}_T) \sim \mathcal{N}(0, \mathbf{I})$, which is formulated as follows,

$$p_\theta(\mathbf{y}_{0:T}|\mathbf{x}) = p(\mathbf{y}_T) \prod_{t=1}^T p_\theta(\mathbf{y}_{t-1}|\mathbf{y}_t, \mathbf{x}), \quad (1)$$

$$p_\theta(\mathbf{y}_{t-1}|\mathbf{y}_t, \mathbf{x}) = \mathcal{N}(\mathbf{y}_{t-1}; \boldsymbol{\mu}_\theta(\mathbf{y}_t, \mathbf{x}, t), \boldsymbol{\Sigma}_\theta(\mathbf{y}_t, \mathbf{x}, t)). \quad (2)$$

The forward process $q(\mathbf{y}_{1:T}|\mathbf{y}_0)$ is defined as a process that progressively involves Gaussian noise into the data according to a variance schedule β_1, \dots, β_T , which is formulated as follows,

$$q(\mathbf{y}_t|\mathbf{y}_{t-1}) = \mathcal{N}(\mathbf{y}_t; \sqrt{1 - \beta_t}\mathbf{y}_{t-1}, \beta_t\mathbf{I}). \quad (3)$$

With the notation $\alpha_t := \prod_{s=1}^t (1 - \beta_s)$, we have

$$q(\mathbf{y}_t|\mathbf{y}_0) = \mathcal{N}(\mathbf{y}_t; \sqrt{\alpha_t}\mathbf{y}_0, (1 - \alpha_t)\mathbf{I}). \quad (4)$$

The conditional DDPM is trained to optimize the upper variational bound on negative log likelihood. Assuming $\boldsymbol{\Sigma}_\theta(\mathbf{y}_t, \mathbf{x}, t)$ as $\sigma_t\mathbf{I}$, the optimization target is equivalent to a denoising process as follows,

$$\mathcal{L}_{t-1} = \mathbb{E}_{\mathbf{y}_0, \epsilon} [\gamma_t \|\epsilon - \epsilon_\theta(\sqrt{\alpha_t}\mathbf{y}_0 + \sqrt{1 - \alpha_t}\epsilon, \mathbf{x}, t)\|_2] \quad (5)$$

where \mathcal{L}_{t-1} is the loss function at the timestep $t - 1$. γ_t is a constant about timestep t .

3.2. Semantic Diffusion Model.

Figure 3 (a) gives an overview of the conditional denoising network in SDM, which is a U-Net-based network estimating the noise in the input noisy image. Unlike previous conditional diffusion models, our denoising network processes the semantic label map and noisy image independently. The noisy image is fed into the denoising network at the encoder part. To fully leverage the semantic information, the semantic label map is injected into the the decoder of the denoising network by multi-layer spatially-adaptive normalization operators.

Encoder. We encode the feature of the noisy image with stacked semantic diffusion encoder resblocks (SDEResblocks) and attention blocks. We show the detailed structure of the SDEResblocks in Figure 3 (b), which consists of convolution, SiLU and group normalization. SiLU [33], which is $f(x) = x \cdot \text{sigmoid}(x)$ simply, is an activation function tending to work better than ReLU [28] on deeper models. To make the network estimate noise at different timestep t , SDEResblock involves t by scaling and shifting the intermediate activation with learnable weight $\mathbf{w}(t) \in \mathbb{R}^{1 \times 1 \times C}$ and bias $\mathbf{b}(t) \in \mathbb{R}^{1 \times 1 \times C}$, which is formulated as follows,

$$\mathbf{f}^{i+1} = \mathbf{w}(t) \cdot \mathbf{f}^i + \mathbf{b}(t), \quad (6)$$

where $\mathbf{f}^i, \mathbf{f}^{i+1} \in \mathbb{R}^{H \times W \times C}$ are the input and output features, respectively. The attention block refer to a self-

attention layer [49] with skip connection, which is formulated as follows,

$$\begin{aligned} \mathbf{f}(\mathbf{x}) &= \mathbf{W}_f \mathbf{x}, \quad \mathbf{g}(\mathbf{x}) = \mathbf{W}_g \mathbf{x}, \quad \mathbf{h}(\mathbf{x}) = \mathbf{W}_h \mathbf{x}, \\ \mathcal{M}(u, v) &= \frac{\mathbf{f}(\mathbf{x}_u)^\top \mathbf{g}(\mathbf{x}_v)}{\|\mathbf{f}(\mathbf{x}_u)\| \|\mathbf{g}(\mathbf{x}_v)\|}, \\ \mathbf{y}_u &= \mathbf{x}_u + \mathbf{W}_v \sum_v \text{softmax}_v(\alpha \mathcal{M}(u, v)) \cdot \mathbf{h}(\mathbf{x}_v), \end{aligned} \quad (7)$$

where \mathbf{x} and \mathbf{y} are the input and output of the attention block. $\mathbf{W}_f, \mathbf{W}_g, \mathbf{W}_h$ and $\mathbf{W}_v \in \mathbb{R}^{C \times C}$ refer to 1×1 convolution in the attention block, respectively. u and v is the index of spatial dimension, range from 1 to $H \times W$. We adopt the attention block on the feature at a specific resolution, *i.e.*, $32 \times 32, 16 \times 16$ and 8×8 .

Decoder. We inject the semantic label map into the decoder of the denoising network to guide the denoising procedure. Revisiting the previous conditional diffusion models [35, 36] which directly concatenate the condition information with the noisy image as input, we find that this approach does not fully leverage the semantic information, which leads to the generated images in low quality and weak semantic relevance. To address this issue, we design the semantic diffusion decoder resblock (SDDResblock) (see Figure 3 (b)) to embed the semantic label map into the the decoder of the denoising network in multi-layer spatially-adaptive manner. Different from SDEResblock, we introduce the spatially-adaptive normalization (SPADE) [31] instead of the group normalization. The SPADE injects the semantic label map into the denoising streams by regulating the feature in a spatially-adaptive, learnable transformation, which is formulated as follows,

$$\mathbf{f}^{i+1} = \gamma^i(\mathbf{x}) \cdot \text{Norm}(\mathbf{f}^i) + \beta^i(\mathbf{x}), \quad (8)$$

where \mathbf{f}^i and \mathbf{f}^{i+1} are the input and output features of SPADE. $\text{Norm}(\cdot)$ refers to the parameter-free group normalization. $\gamma^i(\mathbf{x}), \beta^i(\mathbf{x})$ are the spatially-adaptive weight and bias learned from the semantic layout, respectively. It is worth mentioning that our framework is different from SPADE [31], since our SDM is specifically designed for diffusion process with attention block, skip-connection, and timestep embedding module while SPADE does not.

3.3. Loss functions.

We train our semantic diffusion model with two objective functions. The first objective function is the simple denoising loss. Given a reference output image y and a random timestep $t \in \{0, 1, \dots, T\}$, a noisy version of the reference image \tilde{y} is produced as follows,

$$\tilde{y} = \sqrt{\alpha_t}y + \sqrt{1 - \alpha_t}\epsilon, \quad (9)$$

where ϵ is a noise randomly sampled from the standard Gaussian distribution. α_t is a noise scheduler at timestep

t . We takes T as 1000 in our SDM. The conditional diffusion model is trained to reconstruct the reference image y by predicting the involved noise ϵ under the guidance of the semantic layout x and the timestep t , which is formulated as follows,

$$\mathcal{L}_{\text{simple}} = \mathbb{E}_{t,y,\epsilon} [\|\epsilon - \epsilon_{\theta}(\sqrt{\alpha_t}y + \sqrt{1 - \alpha_t}\epsilon, x, t)\|_2]. \quad (10)$$

Following the improved denoising diffusion model [30], we further train the network to predict variances $\Sigma_{\theta}(\tilde{y}, x, t)$ to improve the log-likelihood of generated images. The conditional diffusion model additionally outputs interpolation coefficient v per dimension and turn the output into variances as follows,

$$\Sigma_{\theta}(\tilde{y}, x, t) = \exp(v \log \beta_t + (1 - v) \log \tilde{\beta}_t) \quad (11)$$

where β_t and $\tilde{\beta}_t$ are the upper and lower bounds on the variance. The second objective function directly optimizes the KL divergence between the estimated distribution $p_{\theta}(\mathbf{y}_{t-1}|\mathbf{y}_t, \mathbf{x})$ and diffusion process posterior $q(\mathbf{y}_{t-1}|\mathbf{y}_t, \mathbf{y}_0)$, which is formulated as follows,

$$\mathcal{L}_{\text{vib}} = \text{KL}(p_{\theta}(\mathbf{y}_{t-1}|\mathbf{y}_t, \mathbf{x})||q(\mathbf{y}_{t-1}|\mathbf{y}_t, \mathbf{y}_0)). \quad (12)$$

In summary, the overall loss is the weighted summation of two objective functions, which is formulated as follows,

$$\mathcal{L} = \mathcal{L}_{\text{simple}} + \lambda \mathcal{L}_{\text{vib}}, \quad (13)$$

where λ is the trade-off parameter to balance loss functions.

3.4. Classifier-free guidance.

Following the common sampling procedure in DDPM, it is noticed that the generated images are diverse but not photo-realistic and not strongly correlated with the semantic label maps. We hypothesis that the conditional diffusion model can not handle conditional input explicitly during the sampling process. Previous method [8] discovered that samples from conditional diffusion models can often be improved by the gradient of the log probability $\nabla_{y_t} \log p(x|y_t)$. Assuming a conditional diffusion model with estimated mean $\mu_{\theta}(y_t|x)$ and variance $\Sigma_{\theta}(y_t|x)$, the results can be improved by perturbing the mean, which is formulated as follows,

$$\hat{\mu}_{\theta}(y_t|x) = \mu_{\theta}(y_t|x) + s \cdot \Sigma_{\theta}(y_t|x) \cdot \nabla_{y_t} \log p(x|y_t) \quad (14)$$

where the hyper-parameter s is named the guidance scale, which trades off the sample quality and diversity.

Previous work [8] applied an extra trained classifier $p_{\phi}(x|y_t)$ to provide the gradient during sampling process. Inspired by [13], we obtain from the guidance with the generative model itself instead of a classifier model that requires extra cost for training. The main idea is to replace the

semantic label map x with a null label \emptyset to disentangle the noise estimated under the guidance of semantic label map $\epsilon_{\theta}(y_t|x)$ from unconditional situation $\epsilon_{\theta}(y_t|\emptyset)$. The disentangled component implicitly infers the gradient of the log probability, which is formulated as follows,

$$\begin{aligned} \epsilon_{\theta}(y_t|x) - \epsilon_{\theta}(y_t|\emptyset) &\propto \nabla_{y_t} \log p(y_t|x) - \nabla_{y_t} \log p(y_t) \\ &\propto \nabla_{y_t} \log p(x|y_t). \end{aligned} \quad (15)$$

During sampling procedure, the disentangled component is increased to improve the samples from conditional diffusion models, which is formulated as follows,

$$\hat{\epsilon}_{\theta}(y_t|x) = \epsilon_{\theta}(y_t|x) + s \cdot (\epsilon_{\theta}(y_t|x) - \epsilon_{\theta}(y_t|\emptyset)). \quad (16)$$

In our implementation, \emptyset is defined as the all-zero vector. We show the detailed sampling procedure in Figure 3 (c).

4. Experiments

4.1. Setup

Datasets. We conduct experiments on four benchmark datasets, *i.e.*, Cityscapes [7], ADE20K [54], CelebAMask-HQ [20] and COCO-Stuff [3]. For Cityscapes dataset, we resize images to the resolution of 256×512 for training. For ADE20K, CelebAMask-HQ and COCO-Stuff dataset, we train our network on the resolution of 256×256 .

Evaluation. We aim to assess visual quality, diversity and learned correspondence of generated images. For the visual quality, we adopt the widely-used Fréchet Inception Distance (FID) metrics. To evaluate the generation diversity of different methods, we compute the average distance measured by the LPIPS metrics [53] between multimodal generation results. For qualitative comparison, we try to compare all the methods but find some models are not publicly available and we also tried to email the author. We then choose the most recent and representative methods whose models are available for testing.

For the learned correspondence, we utilize an off-the-shelf network to evaluate the “semantic interpretability” of generated results. We use DRN-D-105 [52] for Cityscapes, UperNet101 [51] for ADE20K, Unet [20, 34] for CelebAMask-HQ and DeepLabV2 [4] for COCO-Stuff. With the off-the-shelf network, mean Intersection-over-Union (mIoU) is computed based on the generated images and semantic layouts. The mIoU metric refers to the semantic relevance of the generated images. However, mIoU highly depends on the capability of the off-the-shelf network. A strong segmentation network measures the semantic relevance of generated images more correctly. The reported mIoU is calculated by upsampling the generated images to the same resolution as default input resolution of the off-the-shelf segmentation models, which allows a more reasonable evaluation of the semantic interpretability.

Method	CelebAMask-HQ		Cityscapes		ADE20K		COCO-Stuff	
	FID↓	LPIPS↑	FID↓	LPIPS↑	FID↓	LPIPS↑	FID↓	LPIPS↑
Pix2PixHD [48]	38.5	0	95.0	0	81.8	0	111.5	0
SPADE [31]	29.2	0	71.8	0	22.6	0	33.9	0
DAGAN [44]	29.1	0	60.3	0	31.9	0	n/a	0
SCGAN [50]	20.8	0	49.5	0	29.3	0	18.1	0
CLADE [43]	30.6	0	57.2	0	35.4	0	29.2	0
CC-FPSE [24]	n/a	n/a	54.3	0.026	31.7	0.078	19.2	0.098
GroupDNet [57]	25.9	0.365	47.3	0.101	41.7	0.230	n/a	n/a
INADE [42]	21.5	0.415	44.3	0.295	35.2	0.459	n/a	n/a
OASIS [41]	n/a	n/a	47.7	0.327	28.3	0.286	17.0	0.328
SDM(Ours)	18.8	0.422	42.1	0.362	27.5	0.524	15.9	0.518

Table 1. **Quantitative comparison with existing methods on semantic image synthesis.** ↑ indicates the higher the better, while ↓ indicates the lower the better. Notably, our method achieves state-of-the-art performance on FID and LPIPS.

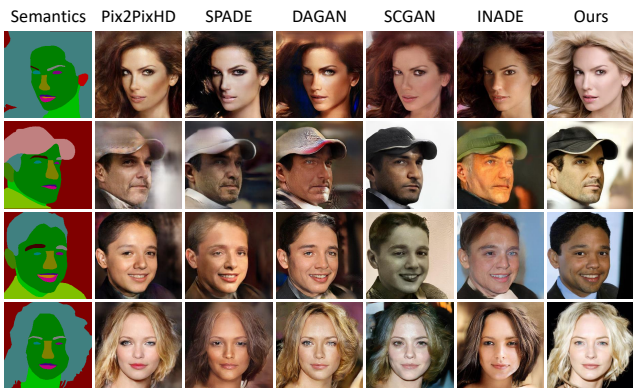


Figure 4. **Qualitative results on the CelebAMask-HQ dataset.** We compared our method with the several challenging methods, *i.e.*, Pix2PixHD [48], SPADE [31], DAGAN [44], SCGAN [50] and INADE [42]. By comparison, our generated images show superior performance on fidelity and learned correspondence, especially on side face situation.

Method	Cityscapes	ADE20K	CelebAMask-HQ	COCO-Stuff
SDM v.s. SPADE	84.0%	87.5%	76.5%	94.0%
SDM v.s. INADE	75.5%	93.5%	89.0%	n/a
SDM v.s. OASIS	84.0%	80.0%	n/a	84.0%

Table 2. Paired user study on four benchmark datasets between our method and several challenging methods, *i.e.*, SPADE [31], INADE [42] and OASIS [41]. The reported numbers refer to the percentage of user preferences in favor of our approach. It is observed that our method is clearly preferred over the competitors on four benchmark datasets.

4.2. Comparison with previous methods

We compare our method with several state-of-the-art methods on semantic image synthesis, *i.e.*, SPADE [31], CC-FPSE [24], INADE [42] and OASIS [41], *etc.*

Key advantages. With the help of progressive refinement of the generated results, our methods achieve superior sample quality to previous GAN-based method. Compared to the most recent methods, our method surpasses them by +2.2, +0.8, +2.0, +1.1 FID score on four datasets, respectively. Besides the quantitative results, we also conduct the qualitative results on four datasets. We show the results in Figure 15, 17 and 7, we observe that the images gen-



Figure 5. **Qualitative results on the ADE20K dataset.** We compare with the several challenging methods, *i.e.*, SPADE [31], CC-FPSE [24], SCGAN [50], INADE [42] and OASIS [41]. By comparison, our method show more reasonable generation results and better exhibit fine-grained details, *i.e.*, water surface and fence.

erated by our method have better visual performance compared with previous methods. Under the complex scenes, *i.e.*, fences in front of the building, human faces in the side view and motorcycles with complex structure, our method can generate samples with more reasonable structure and content, which significantly outperforms previous methods. In Figure 6, we present zoomed-in results of the generated images. Notably, our model exhibits more fine-grained details, such as distant cars and traffic lights.

Furthermore, we conduct a user study to evaluate the visual performance of our method, and three previous methods, *i.e.*, SPADE [31], INADE [42] and OASIS [41]. There are 20 volunteers participating in this study. In the study, we present each volunteer 10 pairs of generated results for each pair user study (100 pairs in total) and ask the volunteers to select more high-fidelity results. The voting results are reported in Table 2. It can be observed that our method is clearly preferred over the competitors in more than 75% of the time on four benchmark datasets.

The other key advantage of our SDM is that our model can inherently generate diverse results given an input semantic mask. We report the results of LPIPS in Table 1, it is observed that our method surpasses the most diverse

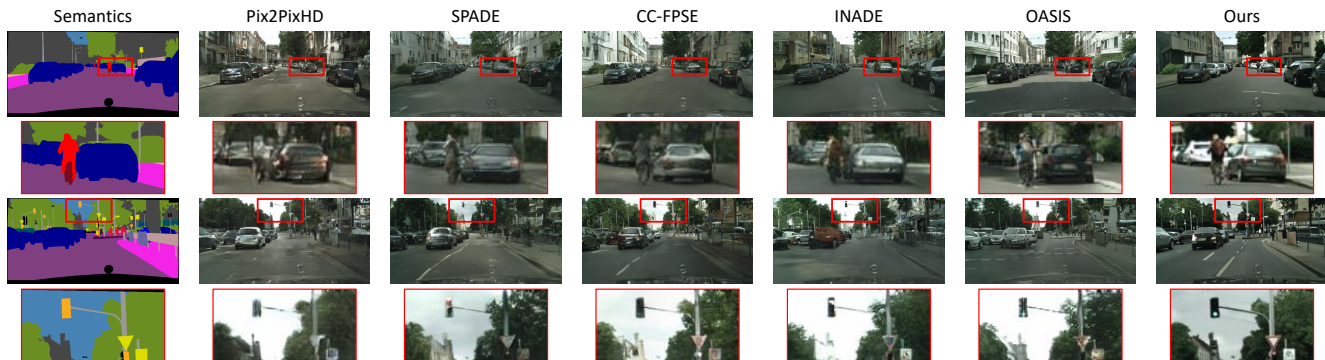


Figure 6. **Qualitative results on Cityscapes datasets.** We compare our method with several challenging methods, *i.e.*, Pix2PixHD [48], SPADE [31], CC-FPSE [24], INADE [42] and OASIS [41]. We present zoomed-in results of the generated images. It is observed that our method generates more reasonable and distinct results on fine-grained objects, such as distant cars and traffic lights.

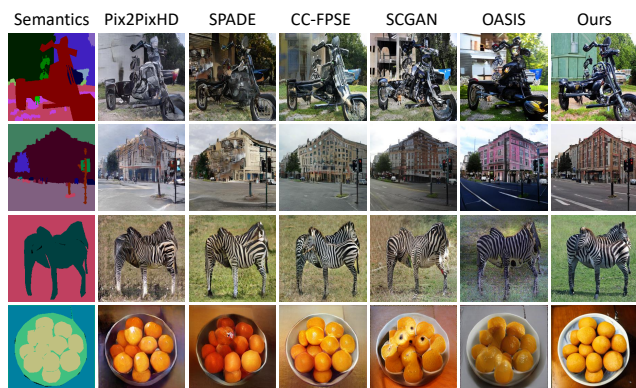


Figure 7. Qualitative results on the COCO-Stuff dataset. We compared our method with the several challenging methods, *i.e.*, Pix2PixHD [48], SPADE [31], CC-FPSE [24], SCGAN [50] and OASIS [41]. By comparison, our method can better generate objects with complex structure, *i.e.*, motorcycle.

Method	CelebAMask	Cityscapes	ADE20K	COCO-Stuff
Pix2PixHD [48]	76.1	63.0	28.8	26.6
SPADE [31]	75.2	61.2	38.3	38.4
DAGAN [44]	76.6	62.4	38.1	n/a
SCGAN [50]	75.5	55.9	41.5	44.3
CLADE [43]	75.4	58.6	23.9	38.8
CC-FPSE [24]	n/a	65.2	40.6	42.9
GroupDNet [57]	76.1	55.3	27.6	n/a
INADE [42]	74.1	57.7	33.0	n/a
OASIS [41]	n/a	58.3	45.7	46.7
SDM (Ours)	77.0	77.5	39.2	40.2

Table 3. mean Intersection-over-Union (mIoU) on four benchmark datasets. The reported mIoU is calculated by upsampling the generated images to the same resolution as default input resolution of the off-the-shelf segmentation models. Among these methods, Pix2PixHD and SPADE on the CelebAMask-HQ dataset are based on our implementation, others are based on released models.

methods by +0.035, +0.065, +0.007, +0.190 LPIPS on four datasets, respectively. Furthermore, we present multimodal generation results in Figure 8, which demonstrates that our method can generate diverse results with high quality.

mIoU comparison and analysis. To evaluate the semantic correspondence, we utilize the mean Intersection-over-

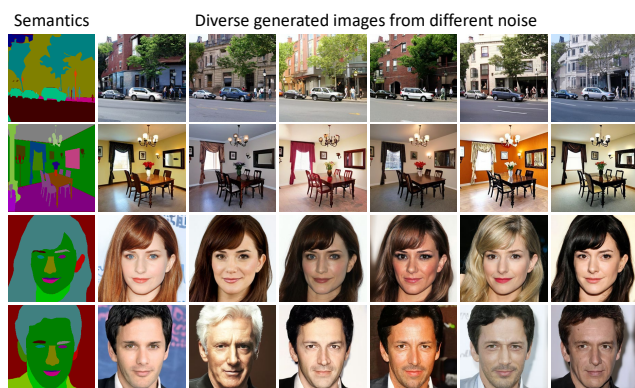


Figure 8. Multimodal generation results from our DDPM-based framework. It is observed that our method can generate diverse results with high quality.

Union (mIoU) with the off-the-shelf segmentation models. On the CelebAMask-HQ and Cityscapes dataset, we achieve 77.0 and 77.5 mIoU, surpassing previous sota by **+0.4** and **+12.3**, indicating the superior performance of our methods for generating highly semantic correlated images. On the ADE20K and COCO-Stuff dataset, our method shows a weaker performance on mIoU compared with some existing methods. However, we observe that our generated images in Figure 17 and 7 have a strong semantic correlation with input mask visually, which are at least comparable with those of previous methods. One possible explanation is that the semantic segmentation model used for evaluating is not that strong, we checked that the segmentation model and find that this model only achieves 35.3 and 39.0 mIoU on the ground-truth images, which is much lower than the model we used on CelebAMask-HQ and Cityscapes dataset. We will show randomly selected 100 results in the supplementary material to further verify this issue.

4.3. Ablation Studies

We perform ablative experiments to verify the effectiveness of several important designs in our framework, *i.e.*, the approach to embed the condition information and the

Settings		Metrics		
w/ SDM structure	w/Guidance	mIoU \uparrow	FID \downarrow	LPIPS \uparrow
×	✓	23.9	39.2	0.508
✓	×	29.7	30.8	0.593
✓	✓	39.2	27.5	0.524

Table 4. Ablation studies on the approach to embed the condition information and the classifier-free guidance strategy. \uparrow indicates the higher the better, while \downarrow indicates the lower the better.



Figure 9. Qualitative results on ablative experiments. The images generated under full settings show superior performance compared with those w/o SDM structure or classifier-free guidance.

classifier-free guidance strategy. We report the qualitative and quantitative results on the ADE20K dataset.

Condition Embedding. To evaluate the importance of embedding the condition information independent of the noisy image, we design a baseline variant as comparison. As an alternative, we directly apply the conditional DDPM in [35,36], which directly concatenates the semantic label map with the noisy image as input. The quantitative results are reported in Table 4. It is observed that our semantic diffusion model highly outperforms previous conditional DDPM on all the metrics. Additionally, we analyze the visual results between these two variants. In Figure 9, it can be seen, by embedding the semantic label map in a multi-layer spatially-adaptive manner, the generated image exhibit superior visual quality on fidelity and correspondence with the semantic label map.

Importance of classifier-free guidance. Furthermore, we study the effectiveness of the classifier-free guidance strategy. We take the variant without classifier-free guidance as a comparison. From Table 4, the classifier-free guidance highly improves the mIoU and FID metrics at the expense of little LPIPS. In Figure 9, we present the qualitative results on the classifier-free guidance strategy. The images generated with classifier-free guidance better exhibit semantic information and generates more structured content. This fur-

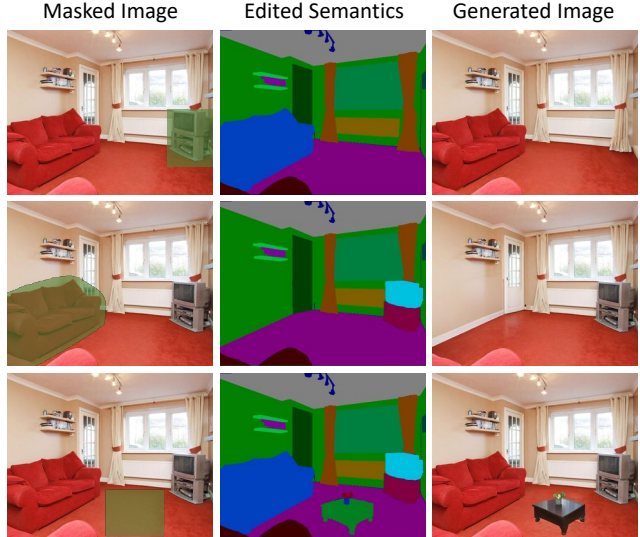


Figure 10. Semantic image editing examples from SDM. The green region is erased, and the model inpaints it based on the edited semantic map. Our model produce a realistic completion matching both the semantic label map and surrounding context.

ther improves the visual effects of generated images compared with those without classifier-free guidance.

4.4. Controlled Generation

We study our semantic diffusion model on the controlled image generation, *i.e.*, semantic image editing. Considering a real image with corresponding semantic label map, we add or remove objects by modifying the semantic label map. After that, the edited region in the real image is erased, and our model inpaints it conditioned on the edited semantic label map. In this way, we can manipulate real images through user interaction. We show the semantic image editing results in Figure 10. It is observed that our model can produce a realistic completion matching both the semantic label map and surrounding context.

5. Conclusions

In this paper, we present the first attempt to explore diffusion model for the problem of semantic image synthesis and design a novel framework named Semantic Diffusion Model (SDM). Specifically, we propose a new network structure to handle noisy input and semantic mask separately and precisely to fully leverage the semantic information. Furthermore, we introduce classifier-free guidance during sampling process, significantly improve the generation quality and semantic interpretability in semantic image synthesis. Extensive experiments on four benchmark datasets demonstrate the effectiveness of our method. Our method achieves state-of-the-art performance in terms of FID and LPIPS metrics and shows better visual quality of generated images compared with previous methods.

References

- [1] Jacob Austin, Daniel Johnson, Jonathan Ho, Daniel Tarlow, and Rianne van den Berg. Structured denoising diffusion models in discrete state-spaces. In *NeurIPS*, volume 34, 2021.
- [2] Omri Avrahami, Dani Lischinski, and Ohad Fried. Blended diffusion for text-driven editing of natural images. *arXiv preprint arXiv:2111.14818*, 2021.
- [3] Holger Caesar, Jasper Uijlings, and Vittorio Ferrari. Cocostuff: Thing and stuff classes in context. In *CVPR*, pages 1209–1218, 2018.
- [4] Liang-Chieh Chen, George Papandreou, Iasonas Kokkinos, Kevin Murphy, and Alan L. Yuille. Semantic image segmentation with deep convolutional nets and fully connected crfs. In *ICLR*, 2015.
- [5] Qifeng Chen and Vladlen Koltun. Photographic image synthesis with cascaded refinement networks. In *ICCV*, pages 1511–1520, 2017.
- [6] Jooyoung Choi, Sungwon Kim, Yonghyun Jeong, Youngjune Gwon, and Sungroh Yoon. Ilvr: Conditioning method for denoising diffusion probabilistic models. *arXiv preprint arXiv:2108.02938*, 2021.
- [7] Marius Cordts, Mohamed Omran, Sebastian Ramos, Timo Rehfeld, Markus Enzweiler, Rodrigo Benenson, Uwe Franke, Stefan Roth, and Bernt Schiele. The cityscapes dataset for semantic urban scene understanding. In *CVPR*, pages 3213–3223, 2016.
- [8] Prafulla Dhariwal and Alex Nichol. Diffusion models beat gans on image synthesis. In *NeurIPS*, volume 34, 2021.
- [9] Ian Goodfellow, Jean Pouget-Abadie, Mehdi Mirza, Bing Xu, David Warde-Farley, Sherjil Ozair, Aaron Courville, and Yoshua Bengio. Generative adversarial nets. In *NeurIPS*, pages 2672–2680, 2014.
- [10] Shuyang Gu, Dong Chen, Jianmin Bao, Fang Wen, Bo Zhang, Dongdong Chen, Lu Yuan, and Baining Guo. Vector quantized diffusion model for text-to-image synthesis. *CVPR*, 2022.
- [11] Jonathan Ho, Ajay Jain, and Pieter Abbeel. Denoising diffusion probabilistic models. In *NeurIPS*, volume 33, pages 6840–6851, 2020.
- [12] Jonathan Ho, Chitwan Saharia, William Chan, David J Fleet, Mohammad Norouzi, and Tim Salimans. Cascaded diffusion models for high fidelity image generation. *Journal of Machine Learning Research*, 23(47):1–33, 2022.
- [13] Jonathan Ho and Tim Salimans. Classifier-free diffusion guidance. In *NeurIPS*, 2021.
- [14] Seunghoon Hong, Dingdong Yang, Yunseok Jang, Tianchen Zhao, and Honglak Lee. Diversity-sensitive conditional generative adversarial networks. In *ICLR*, 2019.
- [15] Kai Katsumata and Hideki Nakayama. Semantic image synthesis from inaccurate and coarse masks. In *ICASSP*, pages 2285–2289, 2021.
- [16] Bahjat Kawar, Michael Elad, Stefano Ermon, and Jiaming Song. Denoising diffusion restoration models. *arXiv preprint arXiv:2201.11793*, 2022.
- [17] Gwanghyun Kim and Jong Chul Ye. Diffusionclip: Text-guided image manipulation using diffusion models. *arXiv preprint arXiv:2110.02711*, 2021.
- [18] Diederik P Kingma, Tim Salimans, Ben Poole, and Jonathan Ho. Variational diffusion models. *arXiv preprint arXiv:2107.00630*, 2021.
- [19] Zhifeng Kong and Wei Ping. On fast sampling of diffusion probabilistic models. *arXiv preprint arXiv:2106.00132*, 2021.
- [20] Cheng-Han Lee, Ziwei Liu, Lingyun Wu, and Ping Luo. Maskgan: Towards diverse and interactive facial image manipulation. In *CVPR*, 2020.
- [21] Haoying Li, Yifan Yang, Meng Chang, Shiqi Chen, Huajun Feng, Zhihai Xu, Qi Li, and Yueting Chen. Srdiff: Single image super-resolution with diffusion probabilistic models. *Neurocomputing*, 2022.
- [22] Ke Li, Tianhao Zhang, and Jitendra Malik. Diverse image synthesis from semantic layouts via conditional imle. In *ICCV*, pages 4220–4229, 2019.
- [23] Yuheng Li, Yijun Li, Jingwan Lu, Eli Shechtman, Yong Jae Lee, and Krishna Kumar Singh. Collaging class-specific gans for semantic image synthesis. In *ICCV*, pages 14418–14427, 2021.
- [24] Xihui Liu, Guojun Yin, Jing Shao, Xiaogang Wang, et al. Learning to predict layout-to-image conditional convolutions for semantic image synthesis. In *NeurIPS*, volume 32, pages 570–580, 2019.
- [25] Jia Long and Hongtao Lu. Generative adversarial networks with bi-directional normalization for semantic image synthesis. In *ICMR*, pages 219–226, 2021.
- [26] Zhengyao Lv, Xiaoming Li, Zhenxing Niu, Bing Cao, and Wangmeng Zuo. Semantic-shape adaptive feature modulation for semantic image synthesis. In *CVPR*, 2022.
- [27] Chenlin Meng, Yang Song, Jiaming Song, Jiajun Wu, Jun-Yan Zhu, and Stefano Ermon. Sdedit: Image synthesis and editing with stochastic differential equations. *arXiv preprint arXiv:2108.01073*, 2021.
- [28] Vinod Nair and Geoffrey E Hinton. Rectified linear units improve restricted boltzmann machines. In *ICML*, 2010.
- [29] Alex Nichol, Prafulla Dhariwal, Aditya Ramesh, Pranav Shyam, Pamela Mishkin, Bob McGrew, Ilya Sutskever, and Mark Chen. Glide: Towards photorealistic image generation and editing with text-guided diffusion models. *arXiv preprint arXiv:2112.10741*, 2021.
- [30] Alexander Quinn Nichol and Prafulla Dhariwal. Improved denoising diffusion probabilistic models. In *ICML*, pages 8162–8171. PMLR, 2021.
- [31] Taesung Park, Ming-Yu Liu, Ting-Chun Wang, and Jun-Yan Zhu. Semantic image synthesis with spatially-adaptive normalization. In *CVPR*, 2019.
- [32] Xiaojuan Qi, Qifeng Chen, Jiaya Jia, and Vladlen Koltun. Semi-parametric image synthesis. In *CVPR*, pages 8808–8816, 2018.
- [33] Prajit Ramachandran, Barret Zoph, and Quoc V Le. Swish: a self-gated activation function. *arXiv preprint arXiv:1710.05941*, 7(1):5, 2017.

- [34] Olaf Ronneberger, Philipp Fischer, and Thomas Brox. U-net: Convolutional networks for biomedical image segmentation. In *MICCAI*, pages 234–241. Springer, 2015.
- [35] Chitwan Saharia, William Chan, Huiwen Chang, Chris A Lee, Jonathan Ho, Tim Salimans, David J Fleet, and Mohammad Norouzi. Palette: Image-to-image diffusion models. *arXiv preprint arXiv:2111.05826*, 2021.
- [36] Chitwan Saharia, Jonathan Ho, William Chan, Tim Salimans, David J Fleet, and Mohammad Norouzi. Image super-resolution via iterative refinement. *arXiv preprint arXiv:2104.07636*, 2021.
- [37] Robin San-Roman, Eliya Nachmani, and Lior Wolf. Noise estimation for generative diffusion models. *arXiv preprint arXiv:2104.02600*, 2021.
- [38] Hiroshi Sasaki, Chris G Willcocks, and Toby P Breckon. Unit-ddpm: Unpaired image translation with denoising diffusion probabilistic models. *arXiv preprint arXiv:2104.05358*, 2021.
- [39] Jascha Sohl-Dickstein, Eric Weiss, Niru Maheswaranathan, and Surya Ganguli. Deep unsupervised learning using nonequilibrium thermodynamics. In *ICML*, pages 2256–2265. PMLR, 2015.
- [40] Jiaming Song, Chenlin Meng, and Stefano Ermon. Denoising diffusion implicit models. In *ICLR*, 2020.
- [41] Vadim Sushko, Edgar Schönfeld, Dan Zhang, Juergen Gall, Bernt Schiele, and Anna Khoreva. You only need adversarial supervision for semantic image synthesis. In *ICLR*, 2021.
- [42] Zhentao Tan, Menglei Chai, Dongdong Chen, Jing Liao, Qi Chu, Bin Liu, Gang Hua, and Nenghai Yu. Diverse semantic image synthesis via probability distribution modeling. In *CVPR*, pages 7962–7971, 2021.
- [43] Zhentao Tan, Dongdong Chen, Qi Chu, Menglei Chai, Jing Liao, Mingming He, Lu Yuan, Gang Hua, and Nenghai Yu. Efficient semantic image synthesis via class-adaptive normalization. *TPAMI*, 2021.
- [44] Hao Tang, Song Bai, and Nicu Sebe. Dual attention gans for semantic image synthesis. In *ACM MM*, pages 1994–2002, 2020.
- [45] Hao Tang, Xiaojuan Qi, Dan Xu, Philip HS Torr, and Nicu Sebe. Edge guided gans with semantic preserving for semantic image synthesis. *arXiv preprint arXiv:2003.13898*, 2020.
- [46] Hao Tang, Dan Xu, Yan Yan, Philip HS Torr, and Nicu Sebe. Local class-specific and global image-level generative adversarial networks for semantic-guided scene generation. In *CVPR*, pages 7870–7879, 2020.
- [47] Min Wang, Congyan Lang, Liqian Liang, Songhe Feng, Tao Wang, and Yutong Gao. Fine-grained semantic image synthesis with object-attention generative adversarial network. *TIST*, 12(5):1–18, 2021.
- [48] Ting-Chun Wang, Ming-Yu Liu, Jun-Yan Zhu, Andrew Tao, Jan Kautz, and Bryan Catanzaro. High-resolution image synthesis and semantic manipulation with conditional gans. In *CVPR*, pages 8798–8807, 2018.
- [49] Xiaolong Wang, Ross Girshick, Abhinav Gupta, and Kaiming He. Non-local neural networks. In *CVPR*, pages 7794–7803, 2018.
- [50] Yi Wang, Lu Qi, Ying-Cong Chen, Xiangyu Zhang, and Ji-aya Jia. Image synthesis via semantic composition. In *ICCV*, pages 13749–13758, 2021.
- [51] Tete Xiao, Yingcheng Liu, Bolei Zhou, Yuning Jiang, and Jian Sun. Unified perceptual parsing for scene understanding. In *ECCV*, 2018.
- [52] Fisher Yu, Vladlen Koltun, and Thomas Funkhouser. Dilated residual networks. In *CVPR*, 2017.
- [53] Richard Zhang, Phillip Isola, and *et al.* The unreasonable effectiveness of deep features as a perceptual metric. In *CVPR*, pages 586–595, 2018.
- [54] Bolei Zhou, Hang Zhao, Xavier Puig, Sanja Fidler, Adela Barriuso, and Antonio Torralba. Scene parsing through ade20k dataset. In *CVPR*, pages 633–641, 2017.
- [55] Jun-Yan Zhu, Richard Zhang, Deepak Pathak, Trevor Darrell, Alexei A Efros, Oliver Wang, and Eli Shechtman. Toward multimodal image-to-image translation. In *NeurIPS*, volume 30, 2017.
- [56] Peihao Zhu, Rameen Abdal, Yipeng Qin, and Peter Wonka. Sean: Image synthesis with semantic region-adaptive normalization. In *CVPR*, pages 5104–5113, 2020.
- [57] Zhen Zhu, Zhiliang Xu, Ansheng You, and Xiang Bai. Semantically multi-modal image synthesis. In *CVPR*, pages 5467–5476, 2020.

This supplementary material provides more details which are not included in the main paper due to space limitations. In the following, we first provide the implementation details. Then we will present more qualitative experiment results.

A. Implementation Details

In this section, we provide more implementation details on the semantic diffusion model, including details on data preprocessing, diffusion procedure, denoising network design, evaluation metrics, hyperparameter and optimization.

Data preprocessing. As mentioned in Section 4.1, we perform experiments on four benchmark datasets, *i.e.*, Cityscapes [7], CelebA-Mask-HQ [20], ADE20K [54], COCO-Stuff [3]. For the Cityscapes dataset, we apply one-hot activation of 35 classes as the input semantic label map. Furthermore, inspired by SPADE [31], we produce an instance edge map from provided instance labels and concatenate it with a semantic label map as additional condition information. The CelebAMask-HQ dataset is processed similarly to the Cityscapes dataset, taking one-hot activation of 19 classes and instance edge map as input. For the ADE20K dataset, we apply one-hot activation of 151 classes (including an “unknown” object) as the input semantic label map. The instance edge map is not employed on ADE20K dataset since the instance labels are not available. On the COCO-Stuff dataset, we utilize one-hot activation of 183 classes (including an “unknown” class) and the instance labels.

Diffusion procedure. As mentioned in Section 3, we propose a semantic diffusion model to transform semantic layouts into realistic images. Following DDPM [11], we set the total diffusion timestep to 1000. In the forward process, the Gaussian noise is involved in the data according to a variance schedule β_1, \dots, β_T . In our implementation, the variance schedule is arranged linearly with respect to the timestep t . During the sampling procedure, we utilize the classifier-free guidance strategy. The classifier-free guidance perturbs the mean as Equation (16) in the main paper. In addition to the mean value, the denoising network also estimates the variance at timestep t , $\Sigma_\theta(\tilde{y}, x, t)$. The variance $\Sigma_\theta(\tilde{y}, x, t)$ is not perturbed in classifier-free guidance.

Since different datasets have different complexity, we apply different guidance scales s on four datasets. Guidance scale s is set to 1.5, 2.0, 1.5 and 1.5 on the CelebAMask-HQ, Cityscapes, ADE20K and COCO-Stuff datasets, respectively. s can affect the trade-off between quality and diversity of generated samples. The probability of dropping labels in classifier-free guidance strategy also affects the performance. We follow [31] and set the probability to 0.2 in the finetune stage by default. We further analyze the performance of different probability setting, *i.e.*, 0.1 and 0.3, on ADE20K dataset. With probabilities set to 0.1 and

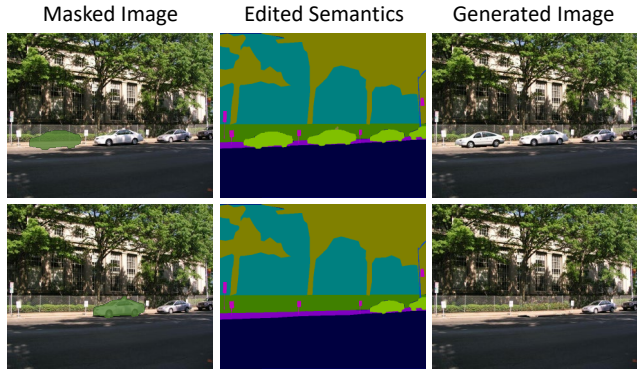


Figure 11. Semantic image editing examples on the street scene from SDM. The green region is edited, and the model inpaints it conditioned on the edited semantic label map.

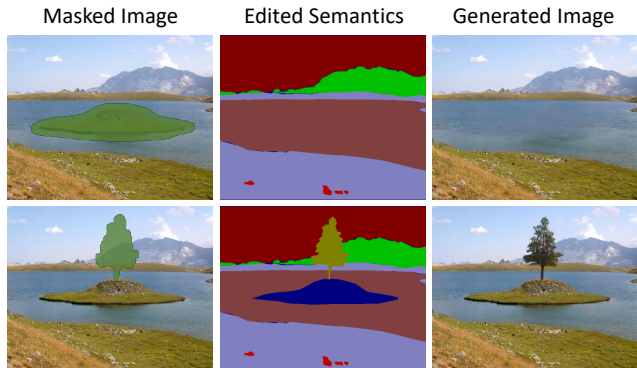


Figure 12. Semantic image editing examples on the natural scene from SDM. The green region is erased, and the model inpaints it conditioned on the edited semantic label map.

0.3, we achieved 29.1 FID and 37.8 mIOU, 30.0 FID and 37.5 mIOU, respectively. These results are slightly worse or comparable with probability set to 0.2.

Denoising network. In Section 3.2, we introduce the conditional denoising network in SDM, which is a U-Net-based network estimating the noise in the input noisy image. The encoder and decoder of the denoising network are 6 layers and the spatial resolution of the feature on each layer is 256×256 , 128×128 , 64×64 , 32×32 , 16×16 and 8×8 , respectively. The channel of each layer is set to 256, 256, 512, 512, 1024 and 1024, respectively. The attention block is applied on the last 3 layers, *i.e.*, the resolution of 32×32 , 16×16 and 8×8 . We utilize the multi-head self-attention mechanism in our implementation and the number of channels in each head is set to 64. In addition, we use half-precision computation to accelerate training and reduce memory consumption.

Evaluation metrics. We adopt a more reasonable approach to measure the mIOU metric in the main paper. Unlike the results reported in [41] which directly adopt the off-the-shelf segmentation model and test the images on 256×256 resolution (that is inconsistent with the input resolution setting of the segmentation model in the training stage), our

reported mIOU is calculated by upsampling the generated images to the same resolution as the default input resolution of the off-the-shelf segmentation model. It is based on two important reasons. First, the segmentation model is trained on cropped patches from original images, which have different scales and aspect ratios from generated images. Second, [41] trained with a discriminative segmentation model on 256×256 , which leads to a bias on 256×256 resolution.

Hyperparameter and Optimization. Following the [30], we set the trade-off parameter λ as 0.001 to ensure training stability. We utilize AdamW optimizer to train the framework. During training, we adopt an exponential moving average (EMA) of the denoising network weights with 0.9999 decay. The whole framework is implemented by Pytorch and the experiments are performed on NVIDIA Tesla V100.

B. Additional Experiment Results

In this section, we first visualize the intermediate results of SDM during the diffusion process. Then we show more generation samples to further demonstrate the effectiveness of our method. Finally, we present more controlled generation results on different scenes to show the robustness of our method.

B.1 Intermediate Results

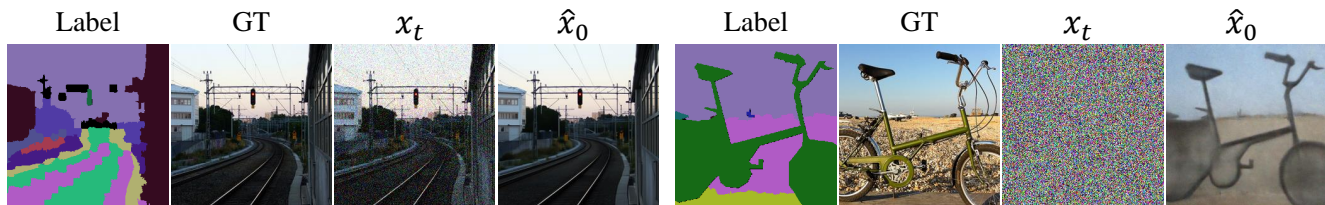
To help readers better understand the entire process of SDM, we visualize the intermediate results in both training and inference procedures. As shown in Figure 13, our method learns to produce noise-free images by predicting the noise involved during the training procedure and generate realistic images with iterative refinement during the inference procedure.

B.2 Generation Samples

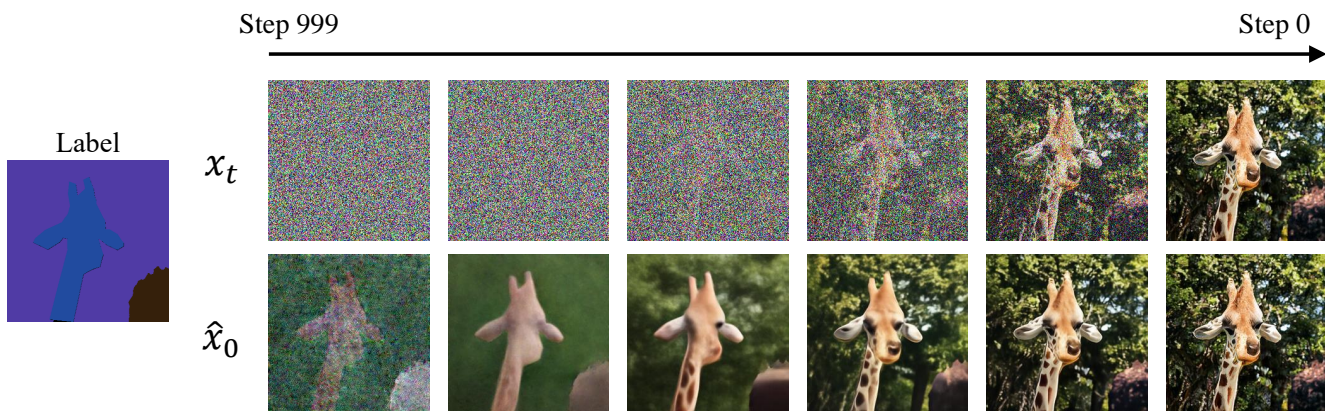
Similar to Section 4.2 of the main paper, we visualize more generation results in Figure 14, 15 and 17. As shown in the figures, our method highly outperforms previous methods on the visual performance of generated images.

B.3 Editing Samples

In the main paper (Section 4.4), we study our semantic diffusion model on controlled image generation. In this section, we further present more semantic image editing results on different scenes in Figure 11 and Figure 12. It demonstrates the robustness of our method on controlled generation, which produces realistic completion matching the semantic label map under different scenes.



(a) Training procedure



(b) Inference procedure

Figure 13. Visualization of the intermediate results in both training and inference procedure. During training, SDM learns to produce noise-free images by predicting the noise involved. In the inference process, SDM generates realistic images with iterative refinement.



Figure 14. More Qualitative results on the Cityscapes dataset. We compared our method with several challenging methods, *i.e.*, Pix2PixHD [48], SPADE [31], CC-FPSE [24], INADE [42] and OASIS [41].

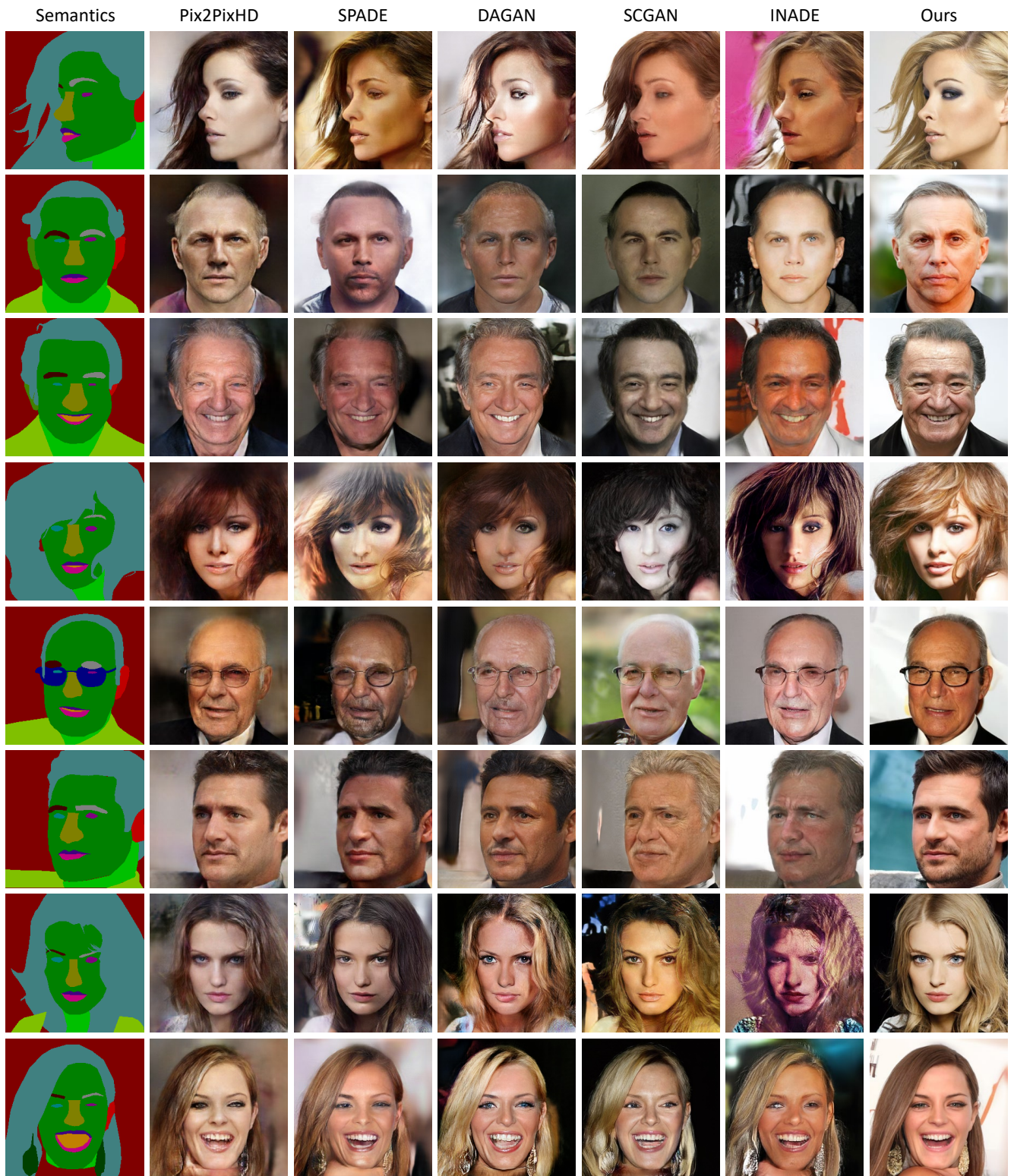


Figure 15. More Qualitative results on the CelebAMask-HQ dataset. We compared our method with several challenging methods, *i.e.*, *i.e.*, Pix2PixHD [48], SPADE [31], DAGAN [44], SCGAN [50] and INAE [42].

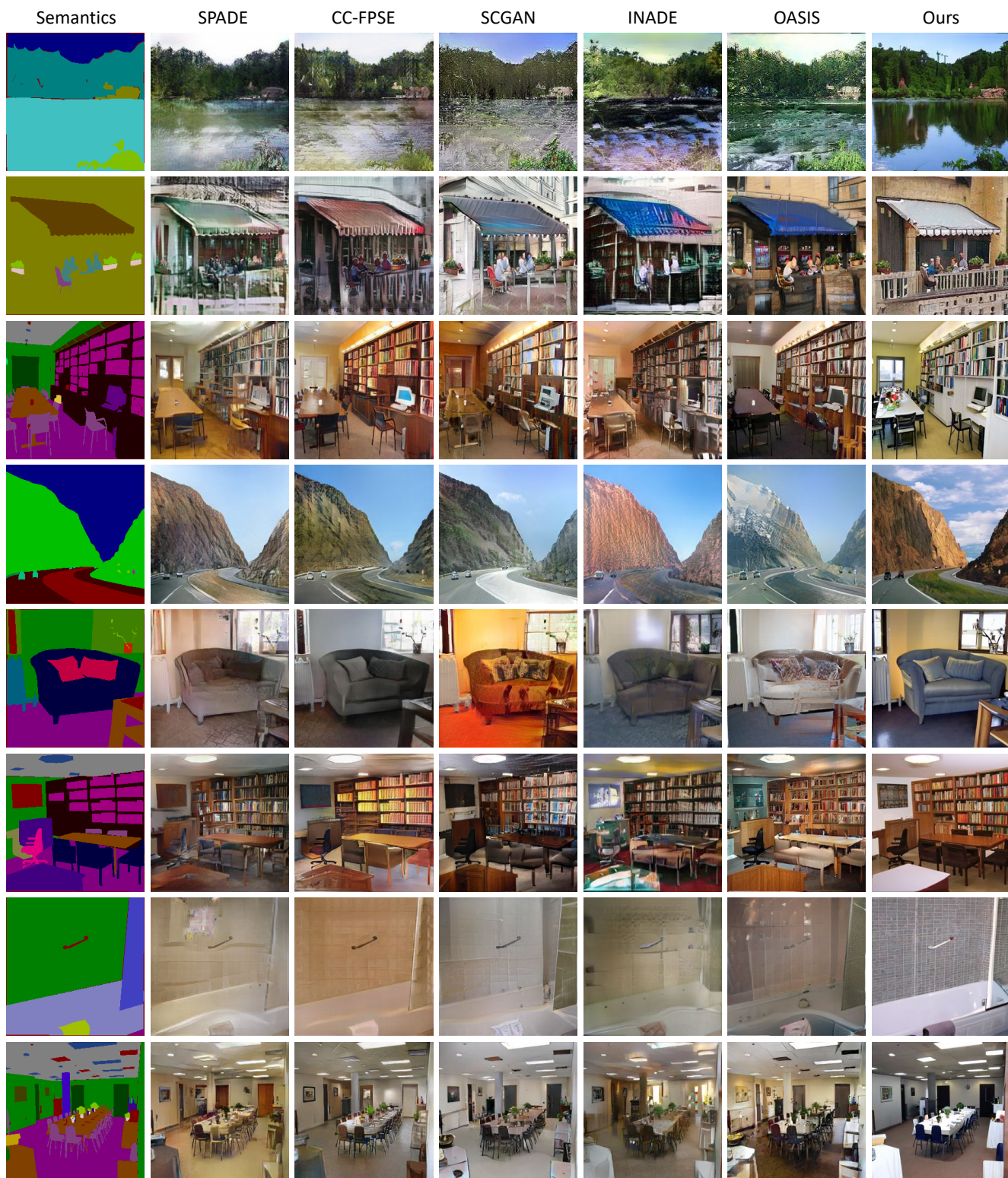


Figure 16. More Qualitative results on the ADE20K dataset. We compared our method with several challenging methods, *i.e.*, SPADE [31], CC-FPSE [24], SCGAN [50], INADE [42] and OASIS [41].

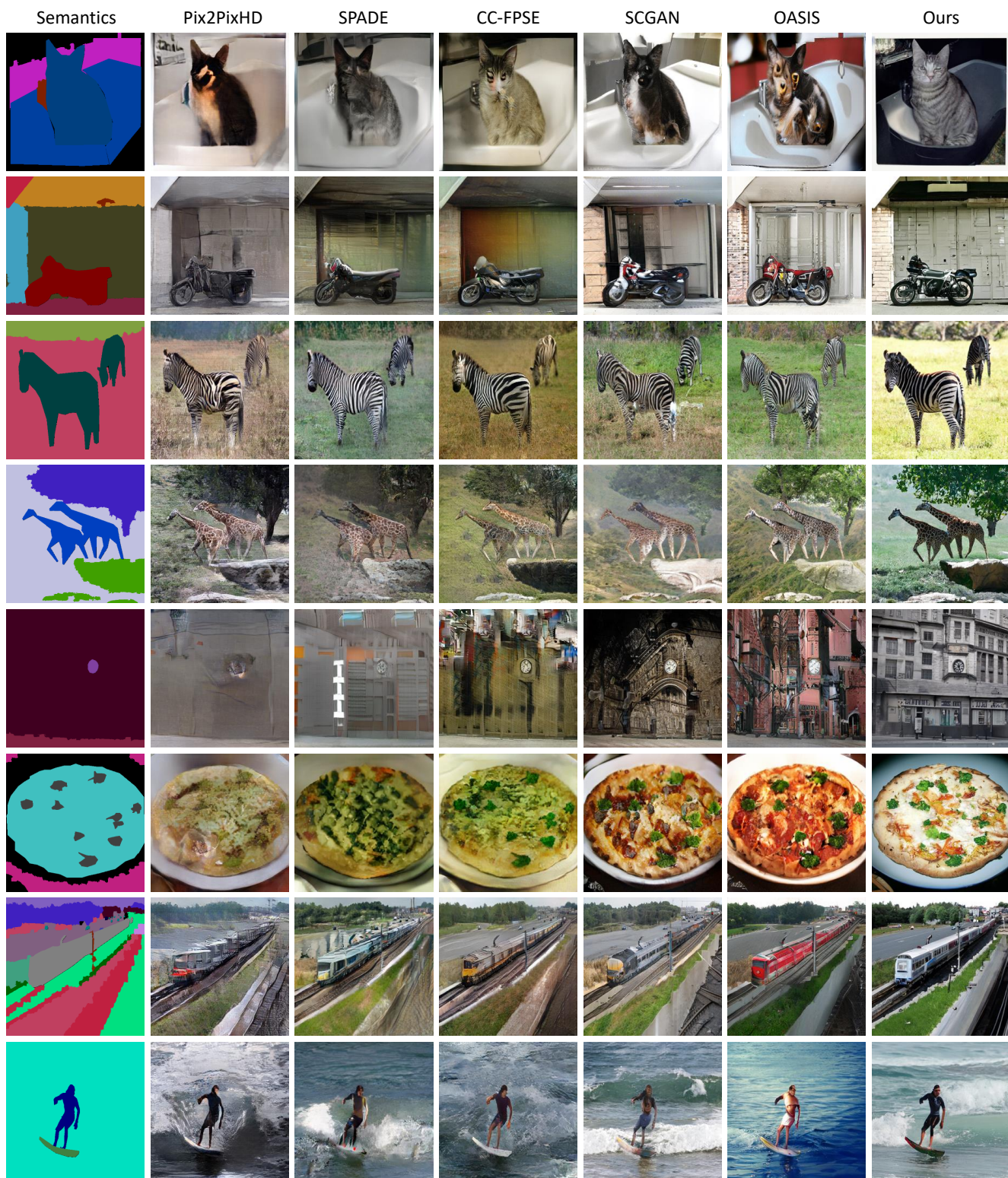


Figure 17. More Qualitative results on the COCO-Stuff dataset. We compared our method with several challenging methods, *i.e.*, Pix2PixHD [48], SPADE [31], CC-FPSE [24], SCGAN [50] and OASIS [41].